SLEEPJ, 2020, 1–16

doi: 10.1093/sleep/zsz189
Advance Access Publication Date: 26 September 2019
Original Article

ORIGINAL ARTICLE

Neuropeptide S promotes wakefulness through the inhibition of sleep-promoting ventrolateral preoptic nucleus neurons

Frédéric Chauveau[1], Damien Claverie[1], Emma Lardant[1], Christophe Varin[2,3], Eléonore Hardy[4], Augustin Walter[4], Frédéric Canini[1,5,†], Nathalie Rouach[4,†] and Armelle Rancillac[2,4,*]

[1]IRBA (Armed Biomedical Research Institute), Brétigny-sur-Orge, France, [2]Brain Plasticity Unit, CNRS, UMR 8249, ESPCI-ParisTech, PSL Research University, Paris 75005, France, [3]Laboratory of Neurophysiology, ULB Neuroscience Institute, Université Libre de Bruxelles (ULB), Brussels, Belgium, [4]Neuroglial Interactions in Cerebral Physiopathology, CIRB, Collège de France, CNRS UMR 7241/Inserm U1050, Labex Memolife, PSL Research University, Paris 75005, France and [5]Ecole du Val de Grâce, 1 Place, Laveran 75005, Paris

[†]Contributed equally to this work.

*Corresponding author. Armelle Rancillac, Neuroglial Interactions in Cerebral Physiopathology, Center for Interdisciplinary Research in Biology – CIRB, CNRS UMR 7241/Inserm U1050, Collège de France, 11, place Marcelin Berthelot, 75005 Paris, France. Email: armelle.rancillac@college-de-france.fr.

Abstract

Study Objectives: The regulation of sleep-wake cycles is crucial for the brain's health and cognitive skills. Among the various substances known to control behavioral states, intraventricular injection of neuropeptide S (NPS) has already been shown to promote wakefulness. However, the NPS signaling pathway remains elusive. In this study, we characterized the effects of NPS in the ventrolateral preoptic nucleus (VLPO) of the hypothalamus, one of the major brain structures regulating non-rapid eye movement (NREM) sleep.

Methods: We combined polysomnographic recordings, vascular reactivity, and patch-clamp recordings in mice VLPO to determine the NPS mode of action.

Results: We demonstrated that a local infusion of NPS bilaterally into the anterior hypothalamus (which includes the VLPO) significantly increases awakening and specifically decreases NREM sleep. Furthermore, we established that NPS application on acute brain slices induces strong and reversible tetrodotoxin (TTX)-sensitive constriction of blood vessels in the VLPO. This effect strongly suggests that the local neuronal network is downregulated in the presence of NPS. At the cellular level, we revealed by electrophysiological recordings and in situ hybridization that NPSR mRNAs are only expressed by non-Gal local GABAergic neurons, which are depolarized by the application of NPS. Simultaneously, we showed that NPS hyperpolarizes sleep-promoting neurons, which is associated with an increased frequency in their spontaneous IPSC inputs.

Conclusion: Altogether, our data reveal that NPS controls local neuronal activity in the VLPO. Following the depolarization of local GABAergic neurons, NPS indirectly provokes feed-forward inhibition onto sleep-promoting neurons, which translates into a decrease in NREM sleep to favor arousal.

Statement of Significance

Using a multidisciplinary approach, we have identified for the first time specific effects of NPS on the ventrolateral preoptic nucleus (VLPO), one of the main structures regulating NREM sleep. Polysomnographic recordings revealed that NPS injection into the VLPO decreases the time spent in NREM sleep, by reducing the duration of NREM sleep episodes. We further demonstrated that NPS receptor mRNAs are highly expressed by GAD^+/Gal^- neurons. Using electrophysiological recordings, we revealed that NPS application in the VLPO induces a feed-forward inhibition on sleep-promoting neurons to indirectly produce their hyperpolarization. Since NPS release is associated with intense stress exposure and can lead to insomnia and post-traumatic stress disorders, the results of this study may provide new therapeutic targets in the treatment of insomnia as well as anxiety symptoms that are observed following stress exposure.

Key words: feed-forward inhibition; GABAergic neurons; NPS; NREM sleep; patch-clamp; polysomnography; neurovascular coupling; VLPO

Submitted: 5 December, 2018; **Revised:** 26 June, 2019

Introduction

Neuropeptide S (NPS) is a 20-amino acid peptide, named after its conserved N-terminus serine residue [1]. NPS is one of the least abundant neuropeptides in the brain and is expressed in only a few brainstem areas [2]. Nevertheless, its G protein-coupled receptor NPSR is widely distributed throughout the brain, suggesting its involvement in numerous functions. Among other roles, the NPS-NPSR system regulates memory processes [3–5], anxiety and stress responses [6–10], and arousal and sleep-wake cycles [6].

Sleep is a universal and essential biological process of animal life. However, the mechanisms that regulate vigilance states still remain poorly understood, and up to about one-third of the population in the Western world suffers from sleep disturbance [11, 12]. Despite the quite recent identification of NPS involvement in regulating vigilance states, only a few studies have focused so far on its specific effects and mechanisms of action. One study has shown that the intracerebroventricular (i.c.v.) injection of NPS induces arousal and reduces all stages of sleep [6]. Following this seminal work, further behavioral and immunological studies highlighted a role for NPS in arousal promotion and non-rapid eye movement (NREM) sleep regulation. Subsequently, the i.c.v. injection of NPS was shown to increase wakefulness and to enhance c-Fos expression, a widely used marker of neuronal activation, in posterior hypothalamic histaminergic and orexinergic neurons [13]. Conversely, the injection of an NPSR antagonist decreases the time spent in wakefulness and specifically increases the time spent in NREM sleep, without affecting rapid eye movement (REM) sleep [14]. Furthermore, studies of humans focusing on nucleotide polymorphisms in the NPSR gene have revealed a significant effect on sleep patterns [15]. Both NPS-IR nerve fibers and NPSR have already been observed in the ventrolateral preoptic nucleus (VLPO) [16], one of the main brain structure that triggers NREM sleep [17–19], suggesting that NPS release in the VLPO could also directly influence NREM sleep. However, the fine mechanism by which NPS specifically modulates NREM sleep remains unclear.

To determine the role of NPS within the VLPO, we used an integrated quadripartite approach combining polysomnographic recordings in freely moving mice, vascular reactivity measurements, patch-clamp recordings and the detection of individual fluorophores. First, we characterized in vivo the effects of NPS on NREM sleep through its bilateral infusion directly into the anterior hypothalamus, including the VLPO. Next, we highlighted the cellular mechanisms underlying NPS effects by applying NPS on VLPO brain slices and recording its vascular effect, as a readout of local network activity. We then used patch-clamp recording on different subsets of VLPO neurons to determine the precise mode of action of NPS on the cellular elements controlling NREM sleep. Lastly, we determined the subcellular localization of NPSR by combining fluorescent in situ hybridization (FISH) and immunolabeling.

Methods

Animals

Male C57B6J mice were used for in vivo experiments (n = 5 mice, 8 to 12 weeks old; Charles River), as well as for recordings of vascular reactivity (n = 8 mice, P30; Charles River), and in situ FISH hybridization (n = 6 mice, P30; Charles River). Male Gal-GFP mice (n = 29 mice, P30) were used for patch-clamp recordings. The Gal-GFP mouse strain used for this research project (STOCK Tg(Gal-EGFP)HX109Gsat/Mmucd, identification number 016342-UCD) was obtained from the Mutant Mouse Regional Resource Center (United States), a NIH-funded strain repository and was donated to the MMRRC by the NINDS-funded GENSAT BAC transgenic project. Dr. N. Heintz, the donating investigator of this Gal-GFP mouse strain, was the first to publish it [20].

Mice settled in the laboratory at least 1 week before experiments to acclimate to their new environment and were housed in a temperature-controlled (20–22°C) and light-tight ventilated cabinets, under a 12-hour light-dark cycle with ad libitum access to food and water. The beginning of the day (lights-on, rest phase) was at 09:00 am (Zeitgeber time 0; ZT-0). The beginning of the night (lights-off, active phase) was at 09:00 pm (ZT-12). Animals involved in in vivo studies arrived in the laboratory at least 2 weeks before surgery and their sleep recording sessions started at ZT-0. Animals used for ex vivo studies were placed in light-tight ventilated cabinets and sacrificed at ZT-0. All animal procedures were conducted in strict compliance with our institutional protocols and were approved by the European Community Council Directive of January 1, 2013 (2010/63/EU) and the local ethics committee (C2EA-59, "Paris Centre et Sud") and local guidelines for the ethical treatment of animal care (Center for Interdisciplinary Research in Biology in College de France, France). The number of animals used in our study was kept to the necessary minimum.

In vivo NPS microinjections into the VLPO and sleep monitoring

C57BL/6J mice were prepared for simultaneous NPS injections into the VLPO and polysomnography as previously described [21]. Briefly, mice were implanted with one bilateral guide cannula (26G; Plastics One) placed 1 mm above the targeted bilateral VLPO (AP: 0.1 mm; ML: 0.7 mm; DV: 4.5 mm [22] for injections and three stainless-steel screws (00-96X1/16, Plastics One) placed over cerebellar cortex, frontal and parietal cortices for EEG recordings. Two silver-wire electrodes were inserted into neck muscles to record EMG activity (787000, AM Systems). Mice had 10 days to recover from surgery. After 3 days of habituation and acclimation to handling, mice were bilaterally injected with either 0.5 µL of 0.9% saline solution (vehicle) or freshly unfrozen 10 µM NPS solution (in 0.5 µL vehicle) using an internal cannula (33G; Plastics One) connected to a 1 µL-Hamilton syringe placed on an injection pump (KD Scientific; 310 plus model). All animals underwent two bilateral injections spaced by 2 days in a randomized order (vehicle or NPS at an infusion flow rate of 0.5 µL/minute). Thus, each animal served as its own control. Injections were performed at ZT-0 under isoflurane brief anesthesia (induction 5%, maintenance 1.5%). Polysomnographic recordings began after complete recovery of sedation (5–10 seconds), for 3 hours after the infusion in the freely moving mice.

Acquired EEG and EMG signals were amplified (Model 3500, AM System), digitalized and collected via a CED interface with Spike2 software (Cambridge Electronic Design) at a sampling frequency of 520.8 Hz. Three vigilance states, wake, NREM sleep, and REM sleep, were scored and quantified offline in 5-second epochs. A minimum of two consecutive epochs were used to score sleep episodes. Waking was detected by a desynchronized

low-amplitude EEG accompanied by a sustained EMG activity with phasic bursts. NREM sleep was distinguished by high-voltage slow waves and the disappearance of phasic muscle activity. REM sleep was signaled by a muscle atonia with decreased EEG amplitude relative to NREM sleep and a regular pronounced theta rhythm. Standard parameters of vigilance states (duration, percentage, number, and duration of episodes) were then calculated. Relative EEG spectral power and frequency peaks were calculated during wake, NREM, and REM stages on artifact-free 5-second EEG epochs. According to three reference methods, epochs were considered as an artifact when at least one value of the signal was missing, or when the absolute variation of the signal slope was greater than 2 μV/ms, or when the absolute value of the signal exceeded 7 SDs of the mean. The EEG power spectral analysis was performed on MATLAB software (Custom script, Mathworks) in each non-artifacted epoch using a Fast Fourier Transform algorithm with Welch estimation (1-second Hamming window and 50% overlap). The following bands were considered: delta, 1–4 Hz; low theta, 4.0–6.5 Hz; high theta, 6.5–9.5 Hz; α, 9.5–12 Hz; β_1, 13–18 Hz; β_2, 18–25 Hz; slow gamma, 25–50 Hz; fast gamma, 50–80 Hz. In each epoch and for each band, the absolute power was calculated from the EEG spectrum as the area under the spectrum curve and the relative power as the ratio of the absolute power under the total power spectrum. When present, the frequency of the maximal peak power of each band was automatically identified using the integrated function of MATLAB.

Preparation of acute VLPO slices

Animals were decapitated at ZT-0. Brains were quickly extracted without removing the meninges, and coronal slices (300 μm thick) were cut as previously described [23, 24]. Individual slices were then placed in a submerged recording chamber maintained at 32°C and perfused with oxygenated artificial cerebrospinal fluid (aCSF) containing (in mM): 130 NaCl; 5 KCl; 2.4 $CaCl_2$; 20 $NaHCO_3$; 1.25 KH_2PO_4; 1.3 $MgSO_4$; 10 d-glucose and 15 sucrose; (pH = 7.35) and placed under an upright microscope (Zeiss) equipped with a CCD camera (Hamamatsu) for blood vessel recordings or a coolSNAP HQ_2 (Photometrics) for patch-clamp recordings.

Vascular reactivity

300-μm thick slices were placed under the objective of the microscope, maintained at 32°C and perfused at 1–2 mL/minute with oxygenated aCSF. Blood vessels located in the VLPO placed within the focal plane and exhibiting a well-defined luminal diameter (10–20 μm) were selected for vascular reactivity study. Images of blood vessels were acquired every 30 seconds with the Media Cybernetics software. The possible drift of images during the recording time was corrected either on-line for the z-drift or offline for the x and y axes using Image Pro Plus 7.0. Manual replacement of images to minimize the differences between two consecutive frames was performed using a subtraction tool from Image Pro Plus. In order to determine the location of most movements, luminal diameters were quantified at different locations along the blood vessel using custom written routines running within IgorPro (Wavemetrics). Control baselines were recorded for 5 minutes at the start of the acquisition, with temperature maintained at 32 ± 1°C. Vessels with unstable baselines (variability higher than 5%) were discarded from the analysis.

Vasomotor responses were subsequently expressed as percentages of the respective mean baseline diameter. NPS was applied during 2 minutes and its effect was measured for 1 minute, either 7.5 minutes after the application onset for vasoconstrictions or after 14 minutes for vasodilations. The effects of pharmacological blocking were then analyzed by performing statistical comparisons between the mean value of the control baseline and the peak effects.

Drugs

NPS receptor agonist (10 μM; PolyPeptide and GeneCust), S-20-Q antagonist (10 μM; PolyPeptide), tetrodotoxin (TTX; 1 μM; Latoxan), and picrotoxin (100 μM; Sigma) were used in this study.

Whole-cell current-clamp recordings

300-μm thick slices were maintained immersed and continuously perfused at 1–2 mL/minute with oxygenated kynurenic acid-free aCSF. Electrophysiological experiments were performed with a MultiClamp700B (Axon Instruments) amplifier connected to an acquisition board (Digidata 1440; Axon Instruments) attached to a computer running the pCLAMP software (Axon Instruments). Membrane potentials, firing frequencies and input resistances were measured over 2-minute periods for baseline (just prior to NPS application), during 50 seconds for the NPS effect (starting 2 minutes after the onset of the drug application), and during 2 minutes for the recovery (between 8–10 minutes after the drug application onset).

Recordings of VLPO neurons were performed in the whole-cell current-clamp configuration with patch-clamp pipettes (3–6 MΩ) filled with an internal solution containing (in mM): 144 K-gluconate; 3 $MgCl_2$; 0.2 EGTA; 10 HEPES (pH 7.2, 285–295 mOsm). For some recordings, biocytin (5%) was added to the internal solution. Current-clamp recordings were made without series resistance compensation and at resting membrane potential, without adjustment of the membrane potential, excepted for the recordings of NPS effects in the presence of picrotoxin, where ~5–10 pA was injected. A short hyperpolarizing current step at the beginning of each sweep was applied to monitor changes in input resistance throughout the recordings. This protocol sometimes triggered low-threshold spikes (LTS). The liquid junction potential of the patch pipette and the perfused extracellular solution was 11 mV and was not applied to the data. Data were rejected if the input resistance changed by more than 25% during the recording of the control period.

Whole-cell voltage-clamp recordings

300-μm thick slices obtained from Gal-GFP mice were maintained immersed as previously described for current-clamp recordings. Spontaneous currents were recorded from fluorescent neurons in voltage-clamp mode at a holding potential of –50 mV, which was less negative than the reversal potential for sIPSCs. Indeed, the pipette solution contained a low concentration of Cl^- (1 mM), resulting in an E_{Cl} of –111 mV. Therefore, inward currents were considered as sEPSCs and outward currents as sIPSCs [24]. Data were filtered at 2 kHz, digitized at 10 kHz

and acquired on-line using the pCLAMP 10 (Clampex) software (Axon Instruments). The recorded currents were subsequently analyzed using the Clampfit program (version 10.2.0.12; Axon Instruments). The threshold for sIPSC and sEPSC detection was set at 7 pA and the automatic detection was verified post hoc by visual inspection. Frequencies and amplitudes were measured over at least a 3-minute period for baseline (just prior to NPS application), 4 minutes for the NPS effect (starting 1 minute after the onset of the drug application) and at least 3 minutes for the recovery (at least 10 minutes after the drug application onset). Only cells displaying a sIPSC frequency > 0.1 Hz were kept for analysis.

Immunofluorescence and confocal microscopy

Free-floating 300-µm slices containing biocytin-filled neurons were fixed by immersion in 4% paraformaldehyde (overnight; 4°C in 0.1 M phosphate buffer). Slices were then rinsed in PBS. Slices were then sequentially incubated in PB containing 1% H_2O_2 in order to quench endogenous peroxidases. For immunofluorescent detection of collagen IV and biocytin-filled neurons, sections were sequentially incubated with the following: (1) goat anti-collagen IV (1:400, Millipore) in PBS containing 0.5% Triton X-100 (PBST) overnight at 4°C; (2) an Alexa Fluor 558-conjugated rabbit anti-goat IgG (1:300, Invitrogen) overnight at 4°C; and (3) Alexa Fluor 488 streptavidin (1:800, Invitrogen) for 2 hours at room temperature. Three 20-minute PBST washes were performed between each incubation step. Sections were rinsed in PB, mounted in Vectashield (Vector) and were observed with a fluorescent microscope (Zeiss). Confocal images were acquired with a Nikon A1R confocal microscope. Z-stacks were imported into NIH ImageJ for analysis.

High-resolution FISH by RNAscope

To visualize in which VLPO cell types the NPSR mRNAs are expressed, colchicine (40 mg in 10 mL saline, 1.5 µL) was injected into the third ventricle (AP: 0.4 mm, ML: 1 mm, DV: 2 mm) of three mice under ketamine-xylazine anesthesia (100 mg/kg and 10 mg/kg respectively, i.p.) and in situ hybridization experiments were performed. The mice were perfused 48 hours later with PBS, and brains were sliced coronally on a cryostat (20 µm).

FISH was performed on frozen brain sections immobilized on a glass slide coated with Cell Tak (Corning, Corning, NY), following the RNAscope procedures (Advanced Cell Diagnostics, Inc., Newark, CA). Hybridization of a probe against the *Bacillus subtilisdihydrodipicolinate* reductase (dapB) gene was used as negative control. Three brains were processed, and one slice/brain from the middle of the VLPO was imaged for each hemisphere. The names of the probes used are provided in the Supplementary Information section.

Statistics

All data are expressed as the mean ± standard error of the mean (SEM) and represented as bar graphs or as plots of individual values with the mean value ± SEM. The statistical significance of the data was assessed using the nonparametric Wilcoxon and Friedman ANOVA tests (Statistica software, Statsoft) according to the relevant conditions. The significance of intracerebral injections of NPS into the VLPO upon vigilance states was determined using a Wilcoxon test. We used this test as each mouse received both NPS and a vehicle solution, randomly one after the other. This nonparametric test was therefore the most appropriate for these matched samples. A Z-test was also used to compare proportions (SigmaStat software). Mann Whitney U-test was used to determine the significance for unpaired and nonparametric values. The Kolmogorov–Smirnov test (K–S test) is a nonparametric test that was used to compare probability distribution of two samples. Significance was set at $p < 0.05$ and expressed as follows: $^{*}p < 0.05$, $^{**}p < 0.01$, $^{***}p < 0.001$. In all cases, n refers to the number of examined neurons.

Results

Bilateral injection of NPS into the VLPO induces wakefulness and decreases NREM sleep

The i.c.v. injection of NPS or its antagonist was previously shown to modulate both arousal and NREM sleep. To determine whether the effects of NPS upon NREM sleep regulation result from an effect in the VLPO or from an indirect effect via neuronal regulation of wake-promoting structures, we performed bilateral injections of NPS into the anterior hypothalamus (including the VLPO), which is one of the main brain region regulating NREM sleep (Figure 1, A and B). These injections were performed at the beginning of the light phase (rest phase, at Zeitgeber time 0; ZT-0), when sleep pressure is high. Each animal randomly received NPS or a vehicle on day 1 and the other solution 2 days later, so that each animal served as its own control. Behavioral effects of NPS were then analyzed for three hours following the injection and were compared to those induced by the vehicle solution (Figure 1D). We found that the NPS effect was brief and mainly altered behavioral states during the first hour only, as assessed by a Friedman ANOVA to investigate the effect of time (Supplementary Table S1). Next, we compared the NPS effect *vs.* vehicle injection for this first hour and observed that NPS significantly modified the total amount of time spent in both NREM sleep and the wake state, although it had no significant effect on REM sleep (Figure 1E). More precisely, NPS injection decreased the time spent in NREM sleep by 78% ($n = 5$, $p < 0.05$, Wilcoxon test; Figure 1E). Out of the five recorded mice, two did not sleep at all during this time frame. This result suggests that, in the VLPO, NPS essentially interferes with sleep stability. Moreover, NPS increased the latency to the first NREM sleep episode (from 26.2 ± 6.3 to 80.3 ± 12.1 minutes; $p < 0.01$, Wilcoxon test; Figure 1C), suggesting that NPS could also impede NREM sleep onset.

We found that the strong decrease in the time spent in NREM sleep observed during the first hour post-NPS injection essentially resulted from NREM sleep episodes that were reduced by 62% ($n = 5$; Wilcoxon test, $p < 0.05$; Figure 1E). Interestingly, NREM sleep episode durations were consecutively significantly increased ($n = 5$; Friedman ANOVA, $\chi^2 = 7.6$, $p < 0.02$, Supplementary Table S1), suggesting that the NREM sleep stages were more consolidated for the second and third hours post-NPS injection, probably as a result of the previous sleep alterations. In contrast, no significant effect was observed regarding the number of NREM sleep episodes for the first hour after NPS injection ($n = 5$; Wilcoxon test, $p > 0.05$; Figure 1E) or for the two subsequent hours post-NPS injection (Friedman ANOVA, $\chi^2 = 3.26$, $p > 0.05$, Supplementary Table S1). Concomitantly, we observed for the

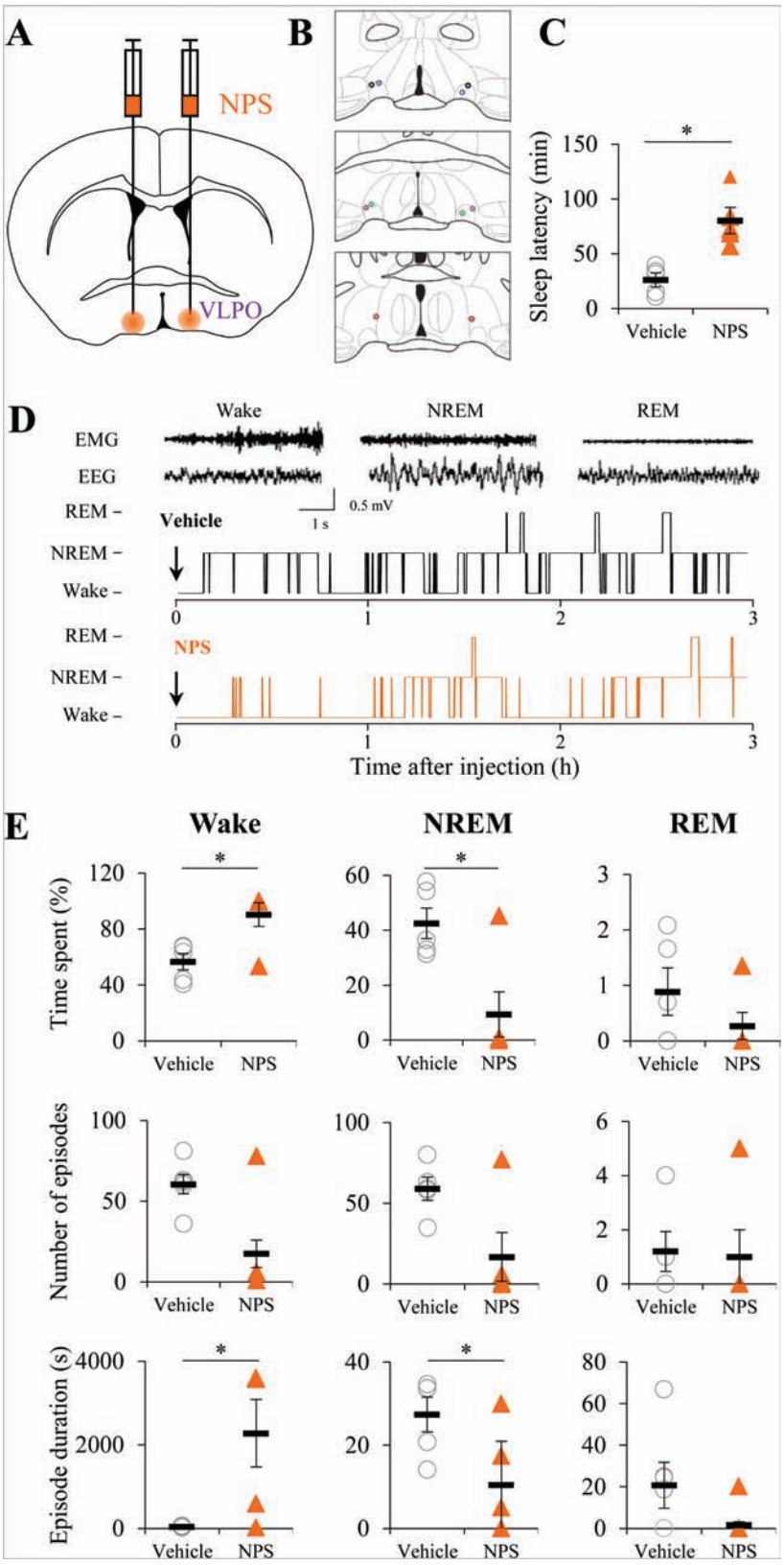

Figure 1. In vivo bilateral NPS infusion in the VLPO promotes wakefulness and decreases NREM sleep. (A) Schematic representation of the injection procedure. (B) Camera lucida drawings of coronal sections showing all injection sites. Black open circles indicate injection sites throughout the rostrocaudal extent of the VLPO, from Bregma 0.14 to –0.22 mm according to the Franklin and Paxinos atlas (2007). (C) Histograms showing the first NREM episode latency ($n = 5$ for both groups). Wilcoxon test: $^{*}p < 0.05$. (D) Typical frontal EEG and EMG raw signals (top panel) and state scoring (5-second epochs) following NPS or vehicle injection in the same mice (bottom panel). (E) Plots of time spent (top panels), the number of episodes (middle panels), and the mean duration of episodes (bottom panels) in response to intra-VLPO injection of NPS (10 µM NPS solution, 0.5 µL per site, $n = 5$) or vehicle solution (0.5 µL, $n = 5$). Data represent the mean value of the first hour after injection.

first hour a 63% increase in the time spent in the wake state after NPS injection (n = 5, Wilcoxon test, $p < 0.05$, Figure 1E).

Spectral analyses of the parietal and frontal derivation for the three behavioral states (wake, NREM, and REM sleep) were performed for the 3 hours following NPS and vehicle injections. Although several mice did not sleep at all during the first hour post-injection of NPS, we observed that during this period, NPS decreased the delta and low theta powers measured at the parietal electrode during NREM sleep (by 54% and 48% respectively, Wilcoxon test, p = 0.10; Supplementary Table S1). The delta and low theta powers measured at the frontal electrode also decreased during the wake period for the first hour after NPS injection (by 34% and 39%, respectively, Wilcoxon test, $p < 0.05$).

These results indicate that local and bilateral administration of NPS into the anterior hypothalamus, including the VLPO, had a short-lasting sleep-suppressing effect, mainly by reducing the mean NREM sleep episode duration.

NPS constricts the blood vessels of the VLPO

Hemodynamic changes are tightly adjusted spatiotemporally to the local neuronal activity of the principal output neurons [25–28]. This neurovascular coupling is regulated by a complex mechanism involving different vasoactive agents released by several cell types [26, 27, 29, 30]. Hemodynamic responses provide an indirect measure of neuronal activity, which can be used to image the activation of brain regions based on their blood oxygenation level-dependent (BOLD) fMRI signal. In the VLPO, sleep-promoting neurons are in tight contact with blood vessels (Figure 2A) and participate in blood flow regulation [30]. Therefore, we used vascular responses as a readout of the local activation of the VLPO neuronal network.

The global effect of NPS on the VLPO neuronal network was determined by applying NPS on brain slices. A 2-minute bath application of NPS induced a strong and reversible vasoconstriction (15.9 ± 0.9%; n = 4; p = 0.001; Wilcoxon test; Figure 2, B and D). This vasoconstriction is likely an indirect result of downregulation of the local neuronal activity, since blood vessels do not express NPSR [1]. The contribution of neurons to the vasoconstrictive effect of NPS was confirmed in slices preincubated with TTX (1 µM), a voltage-gated sodium channel blocker. TTX pretreatment significantly inhibited and even reversed the NPS vasoconstrictive effect. The induced vasodilation developed slowly and peaked at 106.5 ± 2.3% (n = 4; $p < 0.05$; Wilcoxon test; Figure 2, B–D). Typically, vasodilation is measured on preconstricted blood vessels to promote their responsiveness due to the lack of blood pressure in brain slices [26]. Here, the NPS vasodilatory effect under TTX was strong enough to be observed without any vasoconstrictive pretreatment.

Distinct neuronal classes have been characterized in the VLPO according to their morphology, their electrophysiological properties, and their pharmacological responses to neurotransmitters involved in sleep-wake regulation [23, 31]. Two main classes of neurons with a role in sleep-wake regulation have been described: (1) neurons inhibited by noradrenaline (NA), referred to as NA (-) neurons and considered to be putative sleep-promoting neurons; and (2) neurons excited by NA (i.e. NA (+) neurons), which supposedly correspond to local neurons [21, 31–35]. These local GABAergic neurons have already been proposed to regulate the firing of sleep-promoting neurons [36, 37]. Our results suggest that local GABAergic neurons could be directly depolarized by NPS application, mediating the vasodilation observed in the presence of TTX. In contrast, in the absence of TTX, the inhibition of sleep-promoting neurons should induce a strong vasoconstriction that counterbalances the previous vasodilator effect. However, these results do not exclude the fact that other cell types known to regulate cerebral blood flow (such as astrocytes) could also be involved in regulating VLPO neuronal networks. To further decipher the mode of action of NPS on VLPO neuronal subtypes, we next performed ex vivo patch-clamp recordings of neurons in acute brain slices.

NPS hyperpolarizes galaninergic sleep-promoting neurons and depolarizes non-galaninergic neurons in the VLPO

Transgenic mice expressing GFP under the transcriptional control of the galanin gene (Gal-GFP mice) were used to identify putative sleep-promoting neurons in the VLPO, based on the expression of a green fluorescent reporter (Supplementary Figure S1). Indeed, galanin is the only known reliable molecular marker of sleep-promoting cells in the VLPO [38–41]; recently, one elegant study using optogenetic tools also reported that galaninergic neurons in the VLPO promote sleep [42]. In VLPO slices of Gal-GFP mice, Gal-GFP neurons are located in a dense core forming a fluorescent cluster of neurons (Supplementary Figure S1). We established that Gal-GFP VLPO neurons are all inhibited by NA application (50 µM for 20 seconds; n = 14/14; Supplementary Figure S1) and display a potent low-threshold calcium spike, confirming their identification as VLPO sleep-active neurons.

To test the effects of NPS on VLPO neurons, we first investigated whether bath application of NPS could modulate the membrane potential of Gal-GFP neurons using current-clamp recordings. Our results demonstrate that the application of NPS (10 µM for 2 minutes) hyperpolarizes the membrane potential of VLPO neurons by 3.3 ± 0.7 mV (from −49.5 ± 1.8 to −52.8 ± 1.7 mV, n = 8, $p < 0.01$, Wilcoxon test; Figure 3, A, C, and E). Accordingly, spontaneous neuronal firing also significantly decreased by 53% (from 1.1 ± 0.3 to 0.5 ± 0.3 Hz, n = 8, $p < 0.01$, Wilcoxon test; Figure 3D). Additionally, their input resistance was reduced by 7% (from 697 ± 72.1 to 648.3 ± 66.3 MΩ; n = 8, $p < 0.01$, Wilcoxon test; Figure 3F) in response to NPS. All of these effects were reversible.

Since NPSR is a G protein-coupled receptor that couples to either Gq or Gs, the direct effect of linking NPS to its receptor should be a neuronal depolarization, as previously reported in the amygdala [9, 43]. We thus probed whether NPS can inhibit Gal-GFP neurons through the excitation of local GABAergic neurons that have been proposed to control the neuronal activity of sleep-promoting neurons [35, 36]. To test this hypothesis, we recorded the electrophysiological responses of non-Gal-GFP neurons in response to NPS application (10 µM for 2 minutes) within the VLPO. This pharmaceutical NPS application depolarized the membrane potential of non-Gal-GFP neurons by 2.4 ± 0.8 mV (from −55.6 ± 2.4 to −53.2 ± 2.6 mV, n = 7; $p < 0.05$, Wilcoxon test, Figure 3, B, C, and E). Unlike Gal-GFP neurons, non-Gal-GFP neurons rarely fired any spontaneous action potentials at their resting membrane potential (4/7 compared to 8/8). In addition, the neurons in our dataset were 6 mV more hyperpolarized than the Gal-GFP neurons. This indicates that

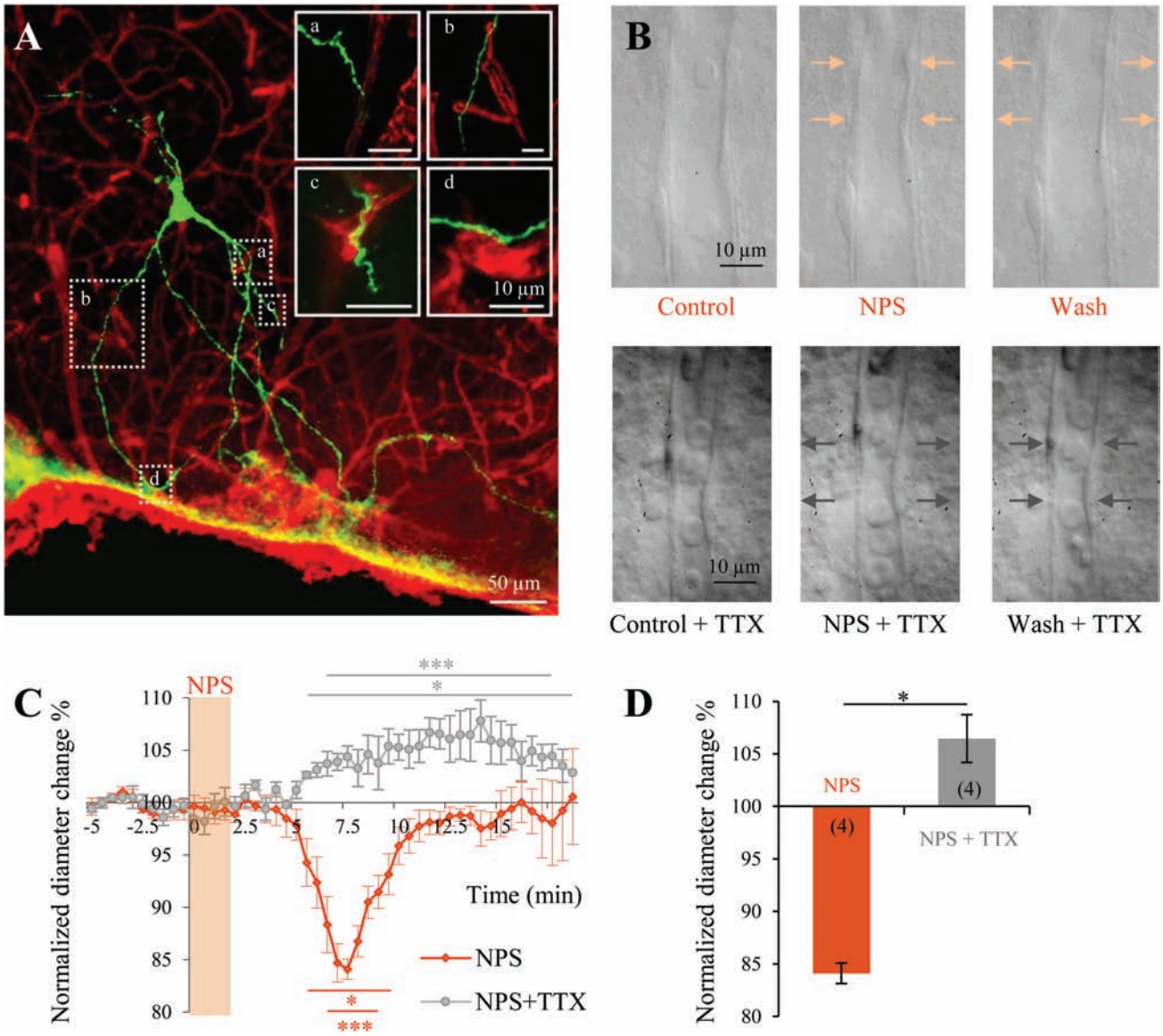

Figure 2. NPS mediates vasoconstriction in the VLPO. (A) Confocal image of a sleep-promoting neuron loaded with biocytin (green), located in the vicinity of blood vessels (immunodetected for collagen IV; red), that was inhibited in response to noradrenalin application. Inserts at the top right are a higher magnification of the region of interest indicated by the white dashed square. (B) Infrared images of a typical vasoconstriction induced by NPS (upper panels), or of a vasodilation induced by NPS application in the presence of TTX (1 µM, bottom panels). The time points are before (control, left panels), at the peak effect (NPS; 2 minutes; 10 µM, middle panels), and during the recovery (wash, right panels). The arrows indicate regions of high vascular reactivity. (C) Mean vascular constrictions induced by NPS (2 minutes; 10 µM; $n = 4$; in orange) and the mean vascular dilation in the presence of TTX (1 µM) induced by NPS (2 minutes; 10 µM; $n = 4$; in gray; $^{*}p < 0.05$, $^{***}p < 0.001$, Wilcoxon tests). (D) Histogram comparing maximal diameter changes induced by NPS either without or under TTX ($^{*}p < 0.05$; Mann Whitey U-test). Sample sizes are indicated in parentheses.

despite our observation that NPS application increases the neuronal firing of non-Gal-GFP neurons (from 0.0 ± 0.0 to 0.5 ± 0.2 Hz, $n = 7$, $p = 0.063$, Wilcoxon test, Figure 3, B and D), this effect was not statistically significant, probably due to the lack of discharge in three out of seven neurons. Nevertheless, a significant 19% decrease in the input resistance was measured while recording the NPS response in Gal-GFP neurons (from 512.4 ± 74 to 412.8 ± 543.5 MΩ; $n = 7$, $p < 0.01$, Wilcoxon test; Figure 3F). Furthermore, the normalized effect of NPS on Gal-GFP neurons was significantly different as compared to the effect on non-Gal-GFP neurons (93.8 ± 1.4 vs. 104.2 ± 1.7 %; $p < 0.001$, Mann-Whitney U-test; Figure 3F). Consequently, NPS may act directly on non-Gal-GFP rather than on Gal-GFP neurons.

NPS indirectly hyperpolarizes Gal-GFP neurons and directly depolarizes non-Gal-GFP neurons

To investigate whether the NPS effect occurs at the pre- or post-synaptic site, we performed bath applications of NPS in the presence of 1 µM TTX, an inhibitor of voltage-sensitive sodium channels, to block indirect neuronal pathways (Figure 4, A, B, and D). In the presence of TTX, we found that NPS application was incapable of changing the membrane potential of Gal-GFP neurons (from –55.1 ± 1.3 to –55.2 ± 1.3 mV; $p = 0.625$, Wilcoxon test; Figure 4, A and C) as well as their input resistance (from 604.6 ± 109.7 to 575.5 ± 105.3 MΩ; $p = 0.188$, Wilcoxon test, Figure 4D). This effect of NPS on membrane potential is significantly different from the

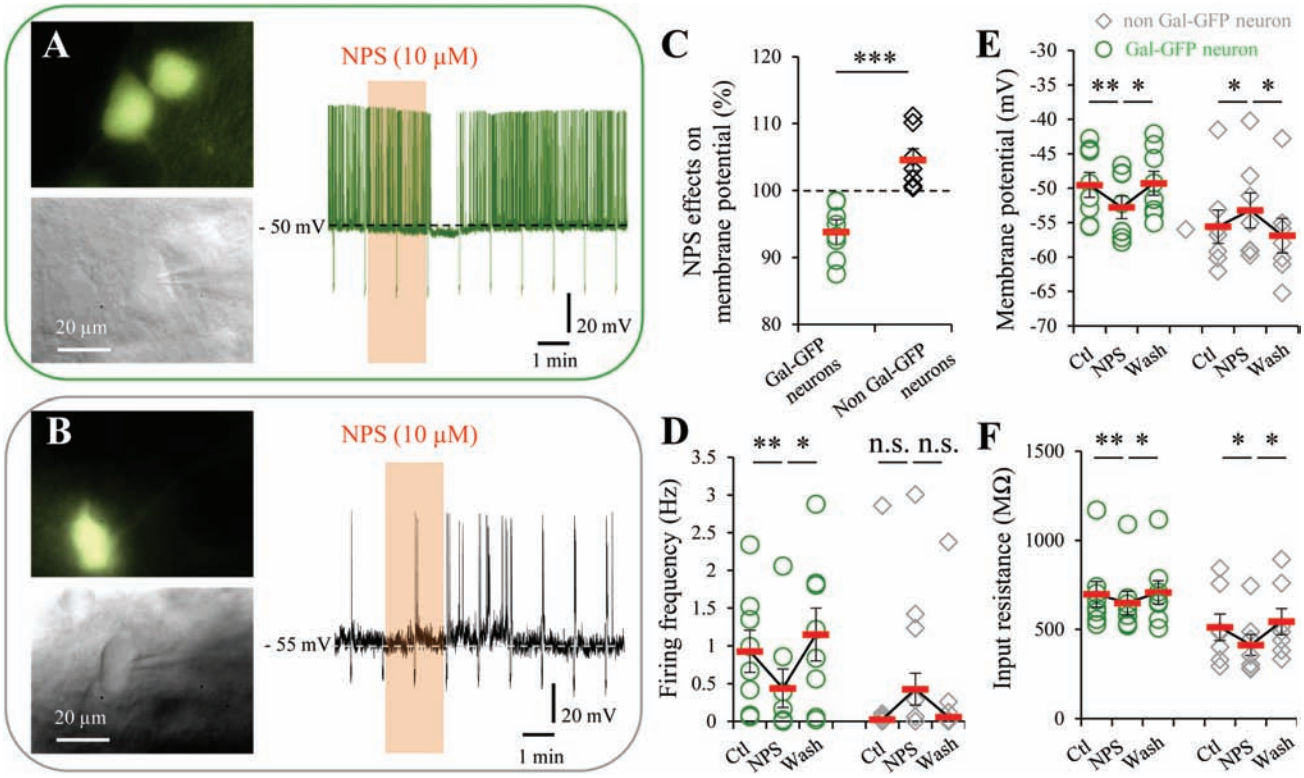

Figure 3. Patch-clamp recordings of neuronal responses to NPS application in the VLPO. (A) Epifluorescence (top left) and infrared (bottom left) images of a Gal-GFP neuron. A sample recording of an individual Gal-GFP neuron in current-clamp mode, at a mean membrane potential of –50 mV (as indicated by the dashed line) is shown. The orange box indicates the duration of NPS application (2 minutes; 10 µM). Hyperpolarizing currents were injected to monitor the input resistance. NPS induced the hyperpolarization of the fluorescent neuron shown in the left panel. (B) Epifluorescence (top) and infrared (bottom) images of a non-Gal-GFP neuron. Same conditions as in (A), but on nonfluorescent neurons and at a mean membrane potential of –55 mV (as indicated by the dashed line). NPS induced the depolarization of the nonfluorescent neuron shown in (B). (C) Summary of NPS effects on the membrane potential of Gal-GFP (green circles, $n = 8$) and non-Gal-GFP neurons (black diamonds, $n = 7$). Empty symbols represent values of individual cells, and solid red bars denote the average values. ***$p < 0.001$; Mann-Whitney U-test. (D–F) Plots of individual membrane variation (D), firing frequency (E), and input resistance (F) of Gal-GFP (green circles, $n = 8$) and non-Gal-GFP neurons (gray diamonds, $n = 7$) in response to NPS application. Solid red bars denote average values. *$p < 0.05$, **$p < 0.001$; Wilcoxon test.

one observed in the absence of TTX (99.7 ± 0.8% vs. 93.8 ± 1.4%; $p < 0.01$, Mann-Whitney U-test, Figure 4F), suggesting an indirect effect of NPS on sleep-promoting neurons.

In contrast, we observed a direct effect of NPS on non-Gal-GFP neurons when the depolarizing effect of bath-applied NPS was maintained in the presence of TTX (Figure 4, B and D). On average, there was a significant membrane potential depolarization of 2.1 ± 0.2 mV (from –56.1 ± 3.8 to –54.7 ± 2.9; $p < 0.05$, Mann-Whitney U-test; Figure 4, B and C), which was not significantly different from the NPS effect without TTX (103.8 ± 0.7% vs. 104.6 ± 1.7%; $p > 0.536$, Mann-Whitney U-test, Figure 4F). The input resistance during recordings of non-Gal-GFP neurons remained sensitive to NPS application under TTX (from 497.1 ± 94.3 to 443.5 ± 103.2 MΩ, $p < 0.05$, Wilcoxon test, Figure 4D).

The specificity of the NPS effect was then tested in the presence of S-20-Q (10 µM), a selective NPSR antagonist. This treatment significantly blocked the expected hyperpolarizing effect of NPS on Gal-GFP neurons (Figure 4, E–G). No significant membrane variation was induced by NPS application in the presence of S-20-Q (from –54.87 ± 1.81 to –53.31 ± 2.61 mV; $n = 6$; $p > 0.62$; Wilcoxon test; Figure 4E). This result was significantly different from the NPS effect without S-20-Q (99.6 ± 0.7% vs. 93.8 ± 0.8%; $p < 0.01$, Mann-Whitney U-test, Figure 4F). In addition, there was no effect of NPS in the presence of S-20-Q, regarding the firing frequency and input resistance (from 0.7 ± 0.3 to 0.5 ± 0.2 Hz; $p = 0.625$; and from 667.1 ± 114.2 to 662.8 ± 188.7 MΩ; $p = 1$, Wilcoxon test; Figure 4, E and G). This set of experiments confirms the involvement of the NPS-NPSR signaling pathway in the hyperpolarizing effect of NPS on Gal-GFP neurons. These results indicate that under physiological conditions, NPS release could first depolarize local non-galaninergic GABAergic neurons, and then mediate a feed-forward inhibition onto sleep-promoting neurons.

NPS specifically increases the frequency of sIPSC input onto Gal-GFP neurons

To test whether the activation of presynaptic NPSR on GABAergic neurons could modulate spontaneous inhibitory (sIPSCs) or excitatory (sEPSCs) inputs onto Gal-GFP neurons, we recorded the spontaneous currents of Gal-GFP neurons in response to NPS application (10 µM, 4 minutes). The corresponding cumulative probability plots for the peak amplitude and interevent intervals of both sIPSCs and sEPSCs revealed that NPS application (10 µM, 4–6 minutes) induced a significant left shift in the cumulative probability distribution of the interevent interval of sIPSCs (K-S test; $p < 0.01$; Figure 5, A–E). Moreover, the mean change of IPSC frequency was significantly increased by 38.4 ± 9.4% in the presence of NPS (Wilcoxon test, $p < 0.01$; Figure 5C; Supplementary Figure S3). Spontaneous EPSCs were only observed in five out of

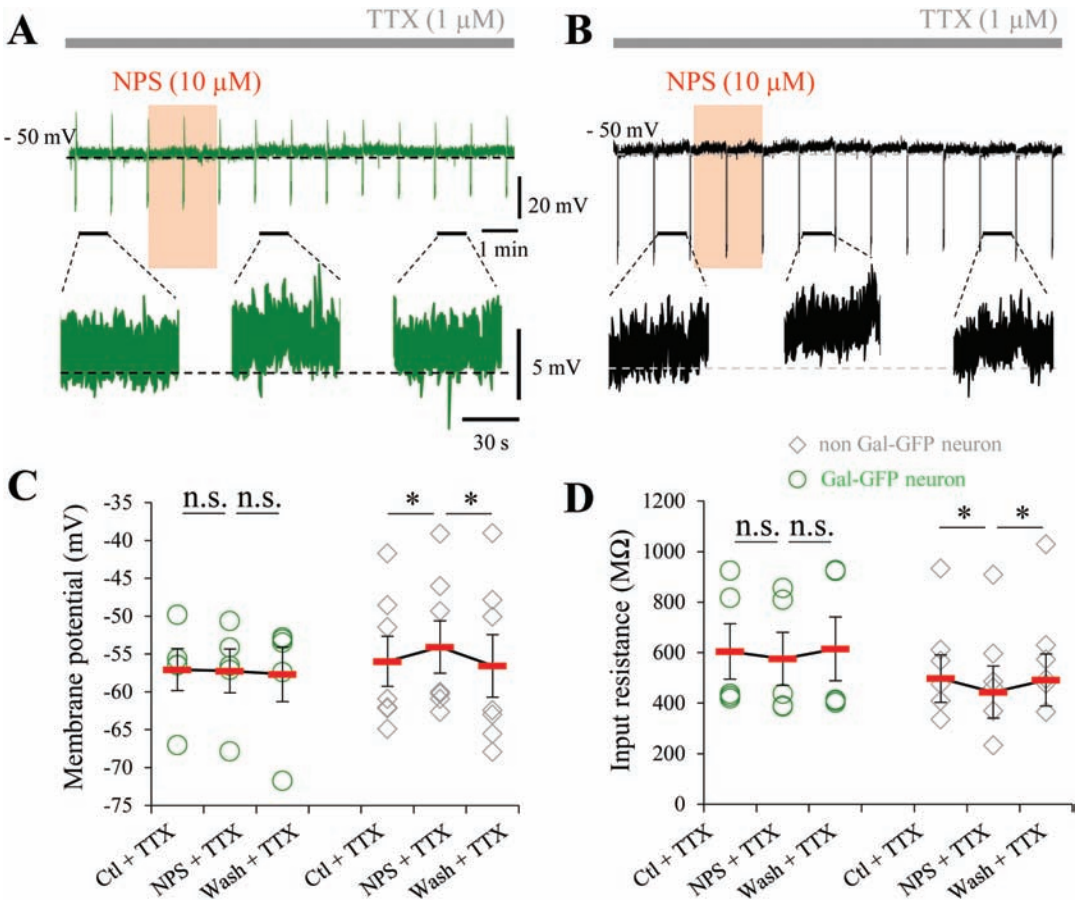

Figure 4. Pharmacological determination of the indirect inhibitory effect of NPS on Gal-GFP neurons. (A) Recording of an individual Gal-GFP neuron in current-clamp mode at a mean membrane potential of –50 mV (as indicated by the dashed line). The recording was performed in the presence of TTX (indicated by the gray bar). The orange box indicates the duration of NPS application (2 minute, 10 µM). Hyperpolarizing currents were injected to monitor the input resistance. Zooms of the recording are represented in the bottom panel. (B) Same conditions as in (A), but on non-Gal-GFP neurons. (C–D) Plots of individual membrane variation (C) and input resistance (D) of Gal-GFP (green circles, $n = 5$) and in non-Gal-GFP neurons (gray diamond; $n = 7$) presence of TTX and in response to NPS application. Solid red bars denote average values. $^{*}p < 0.05$, Wilcoxon test. (E) Same conditions as in (A), but in the presence of the NPSR antagonist S-20-Q (10 µM; orange bar). The hyperpolarizing effect of NPS was occluded by S-20-Q. (F) Summary of NPS effects on the membrane potential of Gal-GFP (in green; $n = 8$ for Gal-GFP neurons, $n = 5$ for Gal-GFP neurons + TTX, and $n = 6$ for GFP neurons + S-20-Q) and non-Gal-GFP neurons (in black; $n = 7$ in each condition). Empty symbols represent the values of individual cells, and solid red bars denote average values. $^{**}p < 0.01$; Mann-Whitney U-test. Note: # indicates the condition where NPS had a significant effect (Wilcoxon test, $\#p < 0.05$). (G) Plots of individual membrane variation (left panel), firing frequency (middle panel), and input resistance (right panel) of Gal-GFP (green circles) in the presence of S-20-Q and in response to NPS application. Solid red bars denote average values. $^{*}p < 0.05$, Wilcoxon test.

six recorded Gal-GFP neurons. We did not observed any significant and reversible effect of NPS on sEPSCs (Figure 5, A, D, and E; Supplementary Figure S3). Individual raw data of NPS effect on sIPSCs and sEPSC variations in frequency and amplitude are represented in Supplementary Figure S3. These results support our hypothesis that the effects of NPS on Gal-GFP neurons could be mediated by the excitation of local non-Gal-GFP, which increases their sIPSC inputs onto sleep-promoting neurons.

NPS hyperpolarizing effect on Gal-GFP neurons is blocked in the presence of a $GABA_A$ receptor antagonist

To determine whether the increase in IPSC frequency induced by NPS could be responsible for the effects seen in VLPO Gal-GFP neurons, the NPS effect was then tested in the presence of picrotoxin (100 µM), a selective GABAA receptor antagonist. We demonstrated that this treatment blocked the hyperpolarizing effect of NPS on Gal-GFP neurons (Figure 5, E and F). No significant membrane variation was induced by NPS application in the presence of picrotoxin (–56.2 ± 0.9 to –56.7 ± 1.1 mV; $n = 6$; $p > 0.699$; Wilcoxon test; Figure 5, E and F). This result was significantly different from the NPS effect obtained in the absence of picrotoxin (99.2 ± 0.8% vs. 93.8 ± 1.7%; $p < 0.01$, Mann-Whitney U-test, Figure 5F). In addition, in the presence of picrotoxin, there was no effect of NPS on the firing frequency and input resistance of sleep-promoting neurons (2.4 ± 0.5 to 2.3 ± 0.6 Hz; $p = 0.699$; and 858.2 ± 69.8 to 855.1 ± 70.6 MΩ; $p = 0.818$, Wilcoxon test; Figure 5G). This experiment supports our hypothesis that NPS may act indirectly on Gal-GFP neurons by regulating afferent GABA release.

Cellular sublocalization of NPSR mRNA

We performed triple FISH experiments on NPSR, GAD and Gal mRNAs within the core of the VLPO to identify the cellular sublocalization of NPSR mRNA expression. Out of 31 $NPSR^+$ cells, only one cell was found co-expressing GAD and Gal (GAD^+/Gal^+ neuron); and 84% (26/31) only co-expressed GAD mRNAs (GAD^+/Gal^- neurons; Figure 6A and Supplementary Figure S2).

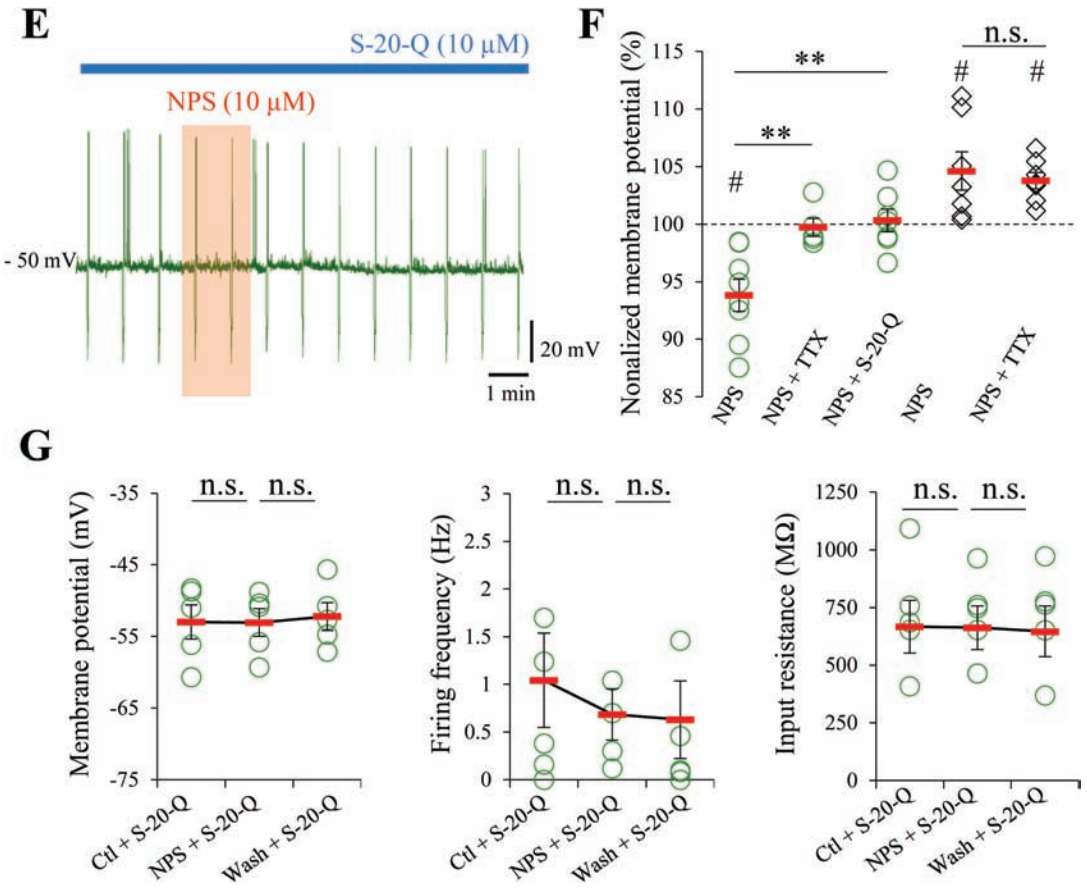

Figure 4. Continued

In addition, only one out of 46 GAD$^+$/Gal$^+$ neurons was NPSR$^+$. Altogether, these data indicate that NPSR mRNAs are primarily expressed by GAD$^+$/Gal$^-$ ($z = 6.145$, $p < 0.001$, Z-test; compared to GAD$^+$/Gal$^+$ neurons; Figure 6A). Furthermore, some NPSR$^+$ expression was observed on GAD$^-$ cells (four out of 31). To further investigate the cellular subtypes expressing this receptor, we performed glial fibrillary acidic protein (GFAP) immunostaining on NPSR and Gal mRNA in situ hybridization. Gal fluorescence confirmed the location within the VLPO. Out of 27 NPSR$^+$ cells, we did not detect any co-expression with GFAP immunolabeling. This allowed us to establish that 0% (0/109) of the astrocytes co-expressed NPSR mRNA (Figure 6B and Supplementary Figure S2), indicating that astrocytes might not have a primary role in the NPS-mediated effect. Altogether, these experiments are in good agreement with our previous electrophysiological results showing a direct effect of NPS on galanin-negative neurons, and an indirect NPS effect on sleep-promoting neurons.

Our study therefore demonstrates for the first time that, within the VLPO, NPS impedes NREM sleep by indirectly inhibiting sleep-promoting neurons. This inhibition of output neurons from the VLPO is associated with a constriction of local blood vessels, reflecting a downregulation of the local network's functional activity (Figure 7).

Discussion

Our study provides the first behavioral, neurovascular and electrophysiological demonstration that NPS decreases NREM sleep by acting in the VLPO. We have shown that NPS has a vasoconstrictive effect, associated with an indirect inhibitory effect on the sleep-promoting neurons. This is an important step in revealing the NPS-responsive circuitry that controls neuronal activity in the VLPO, as well as NREM sleep alteration.

Administration of NPS in the VLPO reduces NREM sleep

Using polysomnographic recordings, we established that the bilateral effects of NPS infusion into the VLPO are transient and highly potent during the first hour, with rapid decreases over the following 2 hours. We observed that NPS increases the time spent awake by 63% and decreases NREM sleep by 78%, through a 62% reduction in NREM sleep episodes.

During the first hour post-injection, NPS strongly reduced the time spent in NREM sleep without altering REM sleep. This could be due to the limited REM sleep amounts during this time period (less than 1%). Alternatively, the NPS awaking effect may specifically target NREM sleep regulation. Our results are in good agreement with previous studies reporting that exogenous NPS promotes wakefulness by decreasing either physiological NREM sleep [6] or pharmacologically induced sleep [44, 45]. Since NREM sleep and wake episode duration in NPS-treated animals are not negatively correlated (data not shown), the present data suggest that NPS locally injected into the anterior hypothalamus decreases NREM sleep by specifically impairing NREM sleep stability. The NREM sleep episode duration consolidation observed during the third hour post-injection is in line with this hypothesis, suggesting the establishment of a compensatory mechanism to overcome the lack of sleep incurred during the first hour.

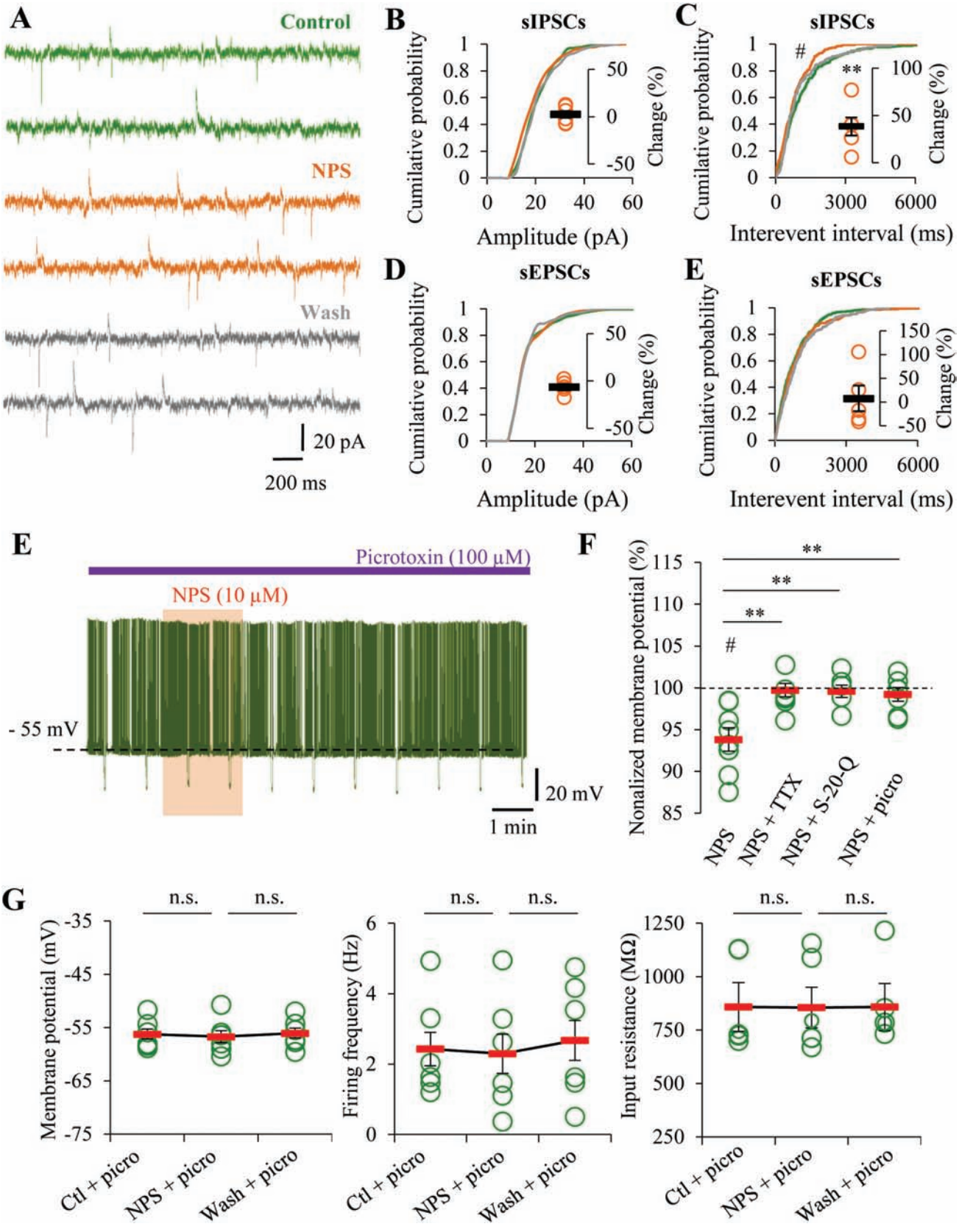

Figure 5. NPS increases the frequency of inhibitory synaptic inputs to Gal-GFP neurons. (A) Representative currents from one cell showing the effect of NPS (10 µM, 4–6 minutes) on sIPSC and sEPSC. The holding potential was set at –50 mV. (B–E) Cumulative probability plots of sIPSC amplitude (B) and interevent interval (D) upon addition of NPS from the cell illustrated in A. Individual plots and averaged amplitude (C) and frequency (E) from all the cells ($n = 5$). (F–I) Same as in B–E but for sEPSC ($n = 4$). Wilcoxon test, $^{*}p \leq 0.05$; K–S test, $\#p \leq 0.05$.

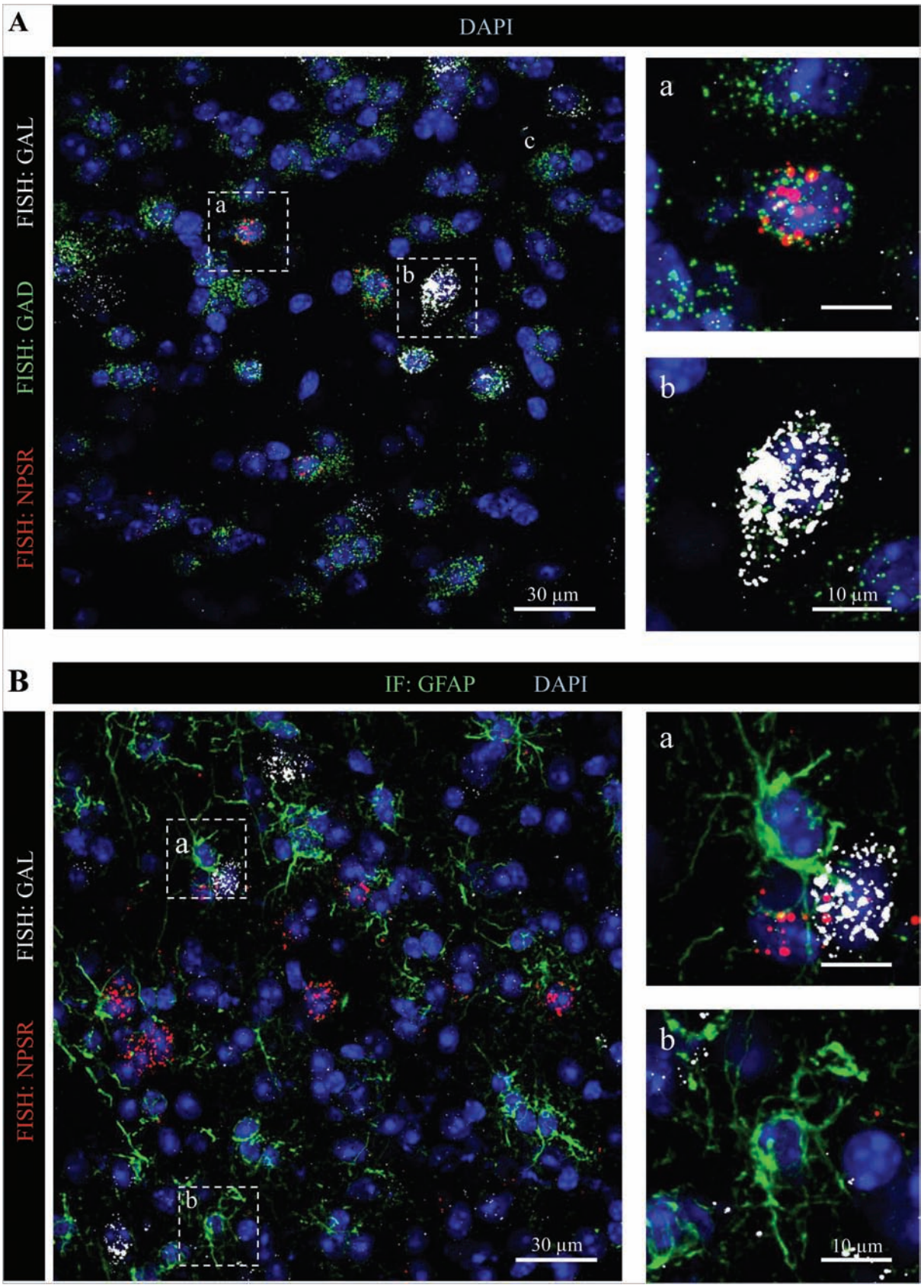

Figure 6. NPSR mRNAs are highly expressed by GAD^{+}/Gal^{-} neurons. (A) Representative confocal images of GAD (green), Gal (white), and NPSR (red) transcripts detected by FISH in VLPO slices. Nuclei were stained with Hoechst stain (blue). (B) Representative confocal images of Gal (white) and NPSR (red) transcripts detected by FISH. Astrocytes were immunostained for GFAP (green), and nuclei were stained with Hoechst stain (blue) in VLPO slices.

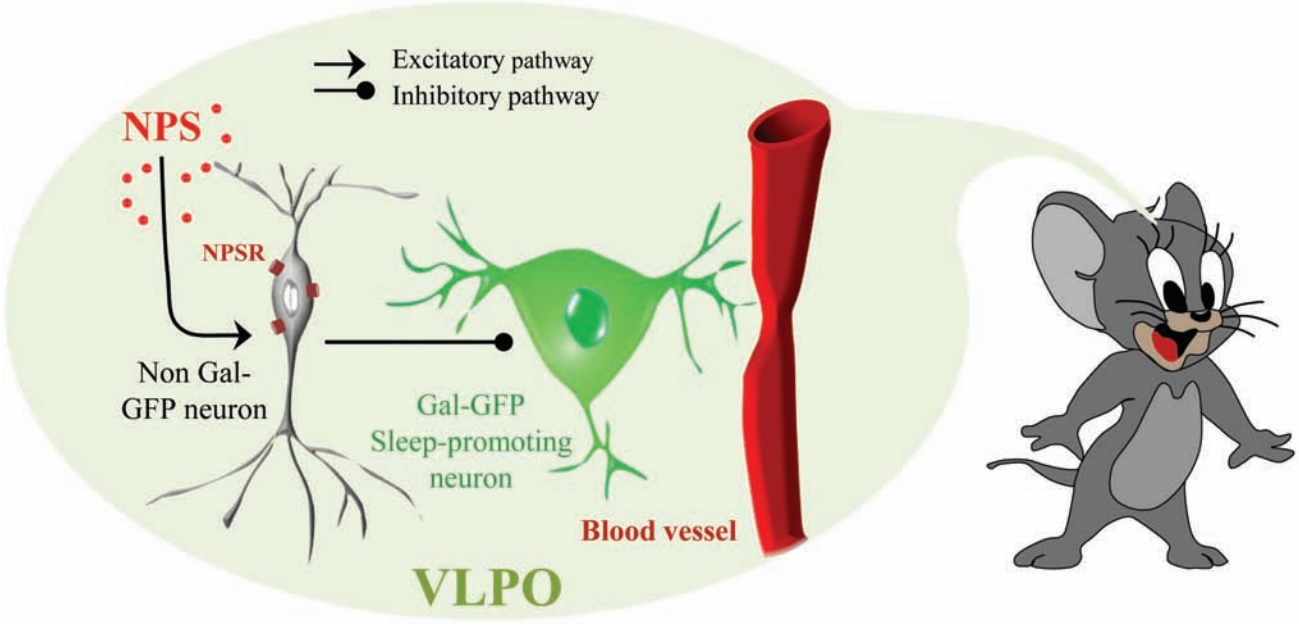

Figure 7. Putative model for how NPS contributes to the maintenance of wakefulness in the VLPO. NPS excites local non-galaninergic neurons, thus decreasing the activity of galaninergic sleep-promoting neurons. The downregulation of sleep-active neurons (i.e. the output neurons of the VLPO) then induces vasoconstriction, which reflects a downregulation of the local neuronal network, possibly promoting wakefulness.

Although NPS infusion did not fully prevent NREM sleep induction and maintenance, two out of five mice showed a total absence of NREM sleep episodes after NPS injection. The observed residual NREM sleep could result from natural activation of other brain structures that are also known to regulate NREM sleep onset. Indeed, the median preoptic nucleus (MnPO) also contains sleep-active neurons that display similar anatomical, physiological, and neurochemical properties as the VLPO neurons [46–48]. Furthermore, the medullary parafacial zone (PZ) also contains GABAergic/glycinergic neurons that are required for natural NREM sleep [49–51]. It has been suggested that VLPO and PZ neurons differentially target features of NREM sleep. The lesioning of either of these structures results in a nearly 50% decrease in NREM sleep. Moreover, VLPO lesions are accompanied by enhanced NREM sleep fragmentation [17], whereas PZ lesions decrease the number of episodes [49]. Here, we observed a strong effect of VLPO activity on the regulation of NREM sleep episode duration. In combination with the decrease in NREM sleep, there was a decrease in delta and low theta power during NREM sleep, which might reflect a lighter sleep state [52]. Regarding the wake state, we found that NPS had no significant effect on beta and gamma power. However, NPS did decrease delta and low theta, suggesting that this treatment favors a cortical arousal state, as previously observed following i.c.v. injection [13, 53]. Altogether, the present data suggest that NPS injection into the VLPO might induce NREM sleep delayed onset and disruption of NREM sleep episodes, leading to a sleep instability that favors arousal.

The NPS mode of action that leads to an enhanced wake state and a decrease in NREM sleep remains incompletely described. However, it is known that when i.c.v. is administered, NPS enhances c-Fos expression in orexinergic and histaminergic neurons of the hypothalamus [13]. These results suggest that the wake-promoting effect of NPS is mediated by the activation of orexinergic and histaminergic neurons. This effect could either be direct, as NPSRs have already been observed in these structures [2, 54], or it could be indirect and reinforced by the new NPS regulatory pathway that we describe in this study. Indeed, we now demonstrate that NPS inhibits the sleep-promoting neurons of the VLPO, a structure that sends inhibitory projections to both orexinergic and histaminergic neurons [41, 55]. NPS could thus act in a cooperative fashion to enhance the excitability of some wake-active systems and inhibit sleep-promoting VLPO neurons. Finally, as NREM sleep regulation is also mediated by PZ neurons, it would be interesting to examine whether simultaneous injections of NPS into the VLPO and the PZ could fully prevent NREM sleep induction and maintenance.

The NPS-NPSR signaling pathway within the VLPO

The cell-specific NPS effects in the VLPO that we described in this study are similar to those that were previously described in the amygdala [9]. Indeed, previous research has identified that NPS controls neuronal activity in the basolateral amygdala via direct action on the endopiriform nucleus, modulating the GABAergic feed-forward inhibition in the basolateral amygdala [43]. Here, we demonstrated in the VLPO that NPS directly excites potent local GABAergic interneurons, thus suggesting that it also indirectly inhibits sleep-promoting neurons. We have indeed shown that NPS decreases the input resistance of non-Gal-GFP neurons by 19%, accompanied by membrane depolarization and increased neuronal firing. Accordingly, we demonstrated that NPS increases the frequency of sIPSCs on sleep-promoting neurons without changing their amplitude, suggesting a presynaptic action for NPS. NPS was also observed to significantly decrease the input resistance of Gal-GFP neurons by 6%, associated with membrane hyperpolarization and decreased neuronal firing. Our finding that the Gal-GFP neuronal firing frequency is higher than in non-Gal-GFP neurons is in good agreement with one of our previous studies, where we determined in cell-attached recordings that NA (-) cells spontaneously discharge at a higher firing rate than NA (+) cells (4.7 ± 0.7 Hz vs. 2.8 ± 0.3 Hz, respectively) [23]. A similar indirect regulation of VLPO

sleep-promoting neuronal activity has been reported for histamine, which depolarizes the membrane potential of the same potent interneurons and ultimately results in the indirect hyperpolarization of sleep-promoting cells [36].

Finally, our FISH results reveal that NPSR mRNAs are preferentially located on local GAD^+/Gal^- neurons, which are depolarized by NPS application. This finding is in line with the previous observation that NPSR activation enhances neuronal excitability [6]. Indeed, NPSR mediates predominantly excitatory signals [56] and is believed to be selectively coupled (with a high affinity) to Gs and Gq protein-couple receptors, increasing intracellular Ca^{2+} and cAMP levels [6, 57]. Therefore, the depolarization of local GABAergic neurons by NPS could increase the frequency of IPSCs on sleep-promoting neurons, leading to their inhibition. Alternatively, since other GABAergic terminals are also present in the VLPO, it might be possible that their stimulation by presynaptic NPSR activation could lead to an increase in IPSC frequency inputs on sleep-promoting neurons, leading to their hyperpolarization. We also demonstrated that in the presence of a $GABA_A$ receptor antagonist, the NPS effects on sleep-promoting neurons were prevented, supporting the hypothesis of a presynaptic action of NPS, that in turn leads to an increased frequency of IPSCs on sleep-promoting neurons, and thereby to their inhibition.

NPS has been well-conserved throughout evolution, suggesting a central role in important physiological functions. For instance, NPS has been shown to be involved in high-stress social interactions. Specifically, NPS release in the amygdala after exposure to an uncontrollable stress results in a submissive behavior [58], which is associated with an anxiolytic effect [59] and the modulation of fear memory [10]. Here, we demonstrated that NPS also regulates the vigilance level.

Hemodynamic responses to NPS within the VLPO also reinforce our hypothesis of a direct action of NPS on local GABAergic neurons and the indirect modulation of the principal cells of the VLPO which are the sleep-promoting neurons. Indeed, it is well accepted that predominant neuronal depolarization corresponds to a local increase in blood flow and oxygenation (i.e. vasodilation), whereas predominant hyperpolarization is associated with a decrease in blood flow and oxygenation (i.e. vasoconstriction) [60, 61]. We have shown that NPS application in the VLPO directly depolarizes local GABAergic neurons to induce a local vasodilation, as revealed in the presence of TTX. However, the subsequent indirect inhibition of sleep-promoting neurons then induces a strong vasoconstriction, reversing the vasodilatory effect induced by the depolarization of NPSR-expressing cells.

Conclusions

The present study identifies a novel direct effect of NPS in the VLPO that decreases the time spent in NREM sleep. This effect reduced episode duration in association with an increase in the time spent in the wake state, mediated by an indirect feed-forward inhibition onto sleep-promoting neurons of the VLPO.

NPS release is associated with an intense stress exposure that leads to insomnia and post-traumatic stress disorders. Therefore, a better determination of the NPR-NPSR signaling pathway could provide new means for identifying the neurobiological processes underlying sleep physiology, which is a prerequisite for developing pharmacological treatments and behavioral strategies to treat sleep dysfunctions.

Supplementary material

Supplementary material is available at *SLEEP* online.

Funding

This work was supported by the Centre National de la Recherche Scientifique (CNRS), the French Institute of Health and Medical Research (Inserm), and the Collège de France. The research work of F.C. was funded by the Direction Générale de l'armement (General Directorate for Armament) (grant number: 12CA703).

Acknowledgments

We thank all members of the animal house facility from Orsay and the Collège de France. We gratefully acknowledge the IT staff, and Aurélien Agneray in particular from the Collège de France, for their excellent and prompt technical assistance. We thank Dr. M. Cohen-Salmon and Marc Oudart for their help and FISH expertise. The authors thank Brandon Loveall from Improvence for English proofreading of the manuscript.
Conflict of interest statement. None declared.

References

1. Xu Y-L, *et al*. Distribution of neuropeptide S Receptor mRNA and neurochemical characteristics of Neuropeptide S-Expressing neurons in the rat brain. *J Comp Neurol*. 2007;**504**(3):287–297.
2. Liu X, *et al*. Molecular fingerprint of neuropeptide S-producing neurons in the mouse brain. *J Comp Neurol*. 2011;**519**(10):1847–1866.
3. Okamura N, *et al*. Neuropeptide S enhances memory during the consolidation phase and interacts with noradrenergic systems in the brain. *Neuropsychopharmacology*. 2011;**36**(4):744–752.
4. Han RW, *et al*. Neuropeptide S facilitates spatial memory and mitigates spatial memory impairment induced by N-methyl-D-aspartate receptor antagonist in mice. *Neurosci Lett*. 2009;**455**(1):74–77.
5. Thomasson J, *et al*. Neuropeptide S overcomes short term memory deficit induced by sleep restriction by increasing prefrontal cortex activity. *Eur Neuropsychopharmacol*. 2017;**27**(12):1308–1318.
6. Xu YL, *et al*. Neuropeptide S: a neuropeptide promoting arousal and anxiolytic-like effects. *Neuron*. 2004;**43**(4):487–497.
7. Leonard SK, *et al*. Pharmacology of neuropeptide S in mice: therapeutic relevance to anxiety disorders. *Psychopharmacology (Berl)*. 2008;**197**(4):601–611.
8. Vitale G, *et al*. Anxiolytic-like effect of neuropeptide S in the rat defensive burying. *Peptides*. 2008;**29**(12):2286–2291.
9. Jüngling K, *et al*. Neuropeptide S-mediated control of fear expression and extinction: role of intercalated GABAergic neurons in the amygdala. *Neuron*. 2008;**59**(2):298–310.
10. Chauveau F, *et al*. Prevention of stress-impaired fear extinction through neuropeptide s action in the lateral amygdala. *Neuropsychopharmacology*. 2012;**37**(7):1588–1599.
11. Chan-Chee C, *et al*. [Epidemiology of insomnia in France]. *Rev Epidemiol Sante Publique*. 2011;**59**(6):409–422.

12. Ford ES, *et al*. Trends in insomnia and excessive daytime sleepiness among U.S. adults from 2002 to 2012. *Sleep Med*. 2015;**16**(3):372–378.
13. Zhao P, *et al*. Neuropeptide S promotes wakefulness through activation of the posterior hypothalamic histaminergic and orexinergic neurons. *Neuroscience*. 2012;**207**:218–226.
14. Oishi M, *et al*. Endogenous neuropeptide S tone influences sleep-wake rhythm in rats. *Neurosci Lett*. 2014;**581**:94–97.
15. Spada J, *et al*. Genetic association of objective sleep phenotypes with a functional polymorphism in the neuropeptide S receptor gene. *PLoS One*. 2014;**9**(6):e98789.
16. Adori C, *et al*. Exploring the role of neuropeptide S in the regulation of arousal: a functional anatomical study. *Brain Struct Funct*. 2016;**221**(7):3521–3546.
17. Lu J, *et al*. Effect of lesions of the ventrolateral preoptic nucleus on NREM and REM sleep. *J Neurosci*. 2000;**20**(10):3830–3842.
18. Sherin JE, *et al*. Activation of ventrolateral preoptic neurons during sleep. *Science*. 1996;**271**(5246):216–219.
19. Szymusiak R, *et al*. Sleep-waking discharge patterns of ventrolateral preoptic/anterior hypothalamic neurons in rats. *Brain Res*. 1998;**803**(1-2):178–188.
20. Gong S, *et al*. A gene expression atlas of the central nervous system based on bacterial artificial chromosomes. *Nature*. 2003;**425**(6961):917–925.
21. Varin C, *et al*. Glucose induces slow-wave sleep by exciting the sleep-promoting neurons in the ventrolateral preoptic nucleus: a new link between sleep and metabolism. *J Neurosci*. 2015;**35**(27):9900–9911.
22. Franklin KBJ, Paxinos G. *The Mouse Brain in Stereotaxic Coordinates,* 3rd edn. San Diego: Academic Press; 2007.
23. Dubourget R, *et al*. Multiparametric characterization of neuronal subpopulations in the ventrolateral preoptic nucleus. *Brain Struct Funct*. 2017;**222**(3):1–15.
24. Sangare A, *et al*. Serotonin differentially modulates excitatory and inhibitory synaptic inputs to putative sleep-promoting neurons of the ventrolateral preoptic nucleus. *Neuropharmacology*. 2016;**109**:29–40.
25. Logothetis NK, *et al*. Neurophysiological investigation of the basis of the fMRI signal. *Nature*. 2001;**412**(6843):150–157.
26. Cauli B, *et al*. Cortical GABA interneurons in neurovascular coupling: relays for subcortical vasoactive pathways. *J Neurosci*. 2004;**24**(41):8940–8949.
27. Rancillac A, *et al*. Glutamatergic control of microvascular tone by distinct GABA neurons in the cerebellum. *J Neurosci*. 2006;**26**(26):6997–7006.
28. Macé E, *et al*. Functional ultrasound imaging of the brain. *Nat Methods*. 2011;**8**(8):662–664.
29. Iadecola C. The Neurovascular unit coming of age: a journey through neurovascular coupling in health and disease. *Neuron*. 2017;**96**(1):17–42.
30. Scharbarg E, *et al*. Astrocyte-derived adenosine is central to the hypnogenic effect of glucose. *Sci Rep*. 2016;**6**:19107.
31. Gallopin T, *et al*. Identification of sleep-promoting neurons in vitro. *Nature*. 2000;**404**(6781):992–995.
32. Liu YW, *et al*. Propofol stimulates noradrenalin-inhibited neurons in the ventrolateral preoptic nucleus by reducing GABAergic inhibition. *Anesth Analg*. 2013;**117**(2):358–363.
33. Moore JT, *et al*. Direct activation of sleep-promoting VLPO neurons by volatile anesthetics contributes to anesthetic hypnosis. *Curr Biol*. 2012;**22**(21):2008–2016.
34. McCarren HS, *et al*. α2-Adrenergic stimulation of the ventrolateral preoptic nucleus destabilizes the anesthetic state. *J Neurosci*. 2014;**34**(49):16385–16396.
35. Matsuo S, *et al*. alpha 2-Adrenoceptor-mediated presynaptic modulation of GABAergic transmission in mechanically dissociated rat ventrolateral preoptic neurons. *J Neurophysiol*. 2003;**89**(3):1640–1648.
36. Liu YW, *et al*. Histamine regulates activities of neurons in the ventrolateral preoptic nucleus. *J Physiol*. 2010;**588**(Pt 21):4103–4116.
37. Williams RH, *et al*. Optogenetic-mediated release of histamine reveals distal and autoregulatory mechanisms for controlling arousal. *J Neurosci*. 2014;**34**(17):6023–6029.
38. Gallopin T, *et al*. The endogenous somnogen adenosine excites a subset of sleep-promoting neurons via A2A receptors in the ventrolateral preoptic nucleus. *Neuroscience*. 2005;**134**(4):1377–1390.
39. Gaus SE, *et al*. Ventrolateral preoptic nucleus contains sleep-active, galaninergic neurons in multiple mammalian species. *Neuroscience*. 2002;**115**(1):285–294.
40. Lu J, *et al*. Selective activation of the extended ventrolateral preoptic nucleus during rapid eye movement sleep. *J Neurosci*. 2002;**22**(11):4568–4576.
41. Sherin JE, *et al*. Innervation of histaminergic tuberomammillary neurons by GABAergic and galaninergic neurons in the ventrolateral preoptic nucleus of the rat. *J Neurosci*. 1998;**18**(12):4705–4721.
42. Kroeger D, *et al*. Galanin neurons in the ventrolateral preoptic area promote sleep and heat loss in mice. *Nat Commun*. 2018;**9**(1):4129.
43. Meis S, *et al*. Identification of a neuropeptide S responsive circuitry shaping amygdala activity via the endopiriform nucleus. *PLoS One*. 2008;**3**(7):e2695.
44. Rizzi A, *et al*. Neuropeptide S is a stimulatory anxiolytic agent: a behavioural study in mice. *Br J Pharmacol*. 2009;**154**(2):471–479.
45. Kushikata T, *et al*. The effects of neuropeptide S on general anesthesia in rats. *Anesth Analg*. 2011;**112**(4):845–849.
46. Gong H, *et al*. Activation of c-fos in GABAergic neurones in the preoptic area during sleep and in response to sleep deprivation. *J Physiol*. 2004;**556**(Pt 3):935–946.
47. Gong H, *et al*. Sleep-related c-Fos protein expression in the preoptic hypothalamus: effects of ambient warming. *Am J Physiol Regul Integr Comp Physiol*. 2000;**279**(6):R2079–R2088.
48. Uschakov A, *et al*. Sleep-active neurons in the preoptic area project to the hypothalamic paraventricular nucleus and perifornical lateral hypothalamus. *Eur J Neurosci*. 2006;**23**(12):3284–3296.
49. Anaclet C, *et al*. The GABAergic parafacial zone is a medullary slow wave sleep-promoting center. *Nat Neurosci*. 2014;**17**(9):1217–1224.
50. Anaclet C, *et al*. Identification and characterization of a sleep-active cell group in the rostral medullary brainstem. *J Neurosci*. 2012;**32**(50):17970–17976.
51. Batini C, *et al*. Presistent patterns of wakefulness in the pretrigeminal midpontine preparation. *Science*. 1958;**128**(3314):30–32.
52. Steriade M. Synchronized activities of coupled oscillators in the cerebral cortex and thalamus at different levels of vigilance. *Cereb Cortex*. 1997;**7**(6):583–604.

53. Ahnaou A, *et al*. Neuropeptide-S evoked arousal with electroencephalogram slow-wave compensatory drive in rats. *Neuropsychobiology*. 2012;**65**(4):195–205.
54. Sutcliffe JG, *et al*. The hypocretins: setting the arousal threshold. *Nat Rev Neurosci*. 2002;**3**(5):339–349.
55. Saito YC, *et al*. GABAergic neurons in the preoptic area send direct inhibitory projections to orexin neurons. *Front Neural Circuits*. 2013;**7**:192.
56. Reinscheid RK, *et al*. Neuropeptide S and its receptor: a newly deorphanized G protein-coupled receptor system. *Neuroscientist*. 2005;**11**(6):532–538.
57. Erdmann F, *et al*. Neuronal expression of the human neuropeptide S receptor NPSR1 identifies NPS-induced calcium signaling pathways. *PLoS One*. 2015;**10**(2):e0117319.
58. Ebner K, *et al*. Increased in vivo release of neuropeptide S in the amygdala of freely moving rats after local depolarisation and emotional stress. *Amino Acids*. 2011;**41**(4):991–996.
59. Wegener G, *et al*. Neuropeptide S alters anxiety, but not depression-like behaviour in flinders sensitive line rats: a genetic animal model of depression. *Int J Neuropsychopharmacol*. 2012;**15**(3):375–387.
60. Wade AR, *et al*. Early suppressive mechanisms and the negative blood oxygenation level-dependent response in human visual cortex. *J Neurosci*. 2010;**30**(14):5008–5019.
61. Devor A, *et al*. Suppressed neuronal activity and concurrent arteriolar vasoconstriction may explain negative blood oxygenation level-dependent signal. *J Neurosci*. 2007;**27**(16):4452–4459.